# Novel cytokinetic ring components limit RhoA activity and contractility

Kathryn Rehain Bell[1,2,3], Michael E. Werner[1,3], Anusha Doshi[1], Daniel B. Cortes[1], Adam Sattler[1], Thanh Vuong-Brender[4], Michel Labouesse[4], Amy Shaub Maddox[1,2,5]

1. Department of Biology, University of North Carolina at Chapel Hill, Chapel Hill, NC, 27599, USA
2. Curriculum in Genetics and Molecular Biology, University of North Carolina at Chapel Hill, Chapel Hill, NC, 27599, USA
3. These authors contributed equally
4. Institut de Biologie Paris-Seine, Sorbonne Université, INSERM, 75005 Paris, France
5. To whom correspondence should be directed; asm@unc.edu

## Abstract

Actomyosin-driven cortical contractility is a hallmark of many biological processes. While most attention has been given to the positive regulation of contractility, it is becoming increasingly appreciated that contractility is also limited by negative regulation and mechanical brakes. The cytokinetic ring is an actomyosin contractile structure whose assembly and constriction are activated by the small GTPase RhoA. Here we describe the role of two novel cytokinetic ring components GCK-1 and CCM-3 in inhibiting contractility in the cytokinetic ring. GCK-1 and CCM-3 co-localize with essential cytokinetic ring proteins such as active RhoA, the scaffold protein anillin and non-muscle myosin II (NMM-II) during anaphase. GCK-1 and CCM-3 are interdependent for their localization and require active RhoA and anillin but not NMM-II for their recruitment to the cytokinetic furrow. Partial depletion of either GCK-1 or CCM-3 leads to an increase of active RhoA, anillin and NMM-II in the cytokinetic furrow and increased rates of furrow ingression. Furthermore, GCK-1 and CCM-3 localize to actomyosin foci during pulsed contractility of the cortical cytoskeleton during zygote polarization. Depletion of GCK-1 or CCM-3 leads to an increase in both cortical contractility and baseline active RhoA levels. Together, our findings suggest that GCK-1 and CCM-3 limit contractility during zygote polarization and

cytokinesis play a more general role in delayed negative feedback regulation of contractile cortical actomyosin networks.

## Introduction

Following faithful replication and segregation of the genome, nascent daughter nuclei are partitioned into individual daughter cells during cytokinesis (Green et al., 2012; Pollard and O'Shaughnessy, 2019). The spatiotemporal coupling of this partitioning with chromosome segregation is achieved by signaling from the anaphase spindle to elicit a zone of active RhoA GTPase at the equatorial cortex (Basant and Glotzer, 2018). RhoA activity initiates a cascade of downstream effects ultimately resulting in the polymerization of filamentous actin (F-actin) and activation of the motor protein non-muscle myosin II (NMM-II). F-actin and NMM-II form the structural basis of the cytokinetic ring along with many other components, including anillin (D'Avino et al., 2015). Anillin binds F-actin, NMM-II, RhoA and other structural and regulatory ring components, thus acting as a scaffold (D'Avino, 2009; Piekny and Maddox, 2010). Once the ring is assembled, it constricts, drawing the plasma membrane into a furrow that partitions the cytoplasm (Cheffings et al., 2016). Complete cytokinetic ring closure is essential for cells to maintain proper ploidy. Failure results in the formation of a polypoid cell that can undergo apoptosis or cancerous transformation (Lacroix and Maddox, 2012).

Despite over 100 years of study, the mechanisms of cytokinetic ring constriction remain poorly understood. To gain new insights, we identified novel anillin-interacting proteins and found Germinal Center Kinase – 1 (GCK-1), a serine/threonine kinase related to budding yeast Ste20 (sterile-20) and the only orthologue of the mammalian germinal center kinase III subfamily in *C. elegans* which have been implicated in apoptosis, proliferation, polarity and cell motility (Rehain-Bell et al., 2017; Schouest et al., 2009; Yin et al., 2012; Zheng et al., 2010). One well characterized

interaction partner of GCK-1 is CCM-3, which is thought to recruit GCK-1 to the STRIPAK complex (Hwang and Pallas, 2014). Together these proteins are thought to regulate endothelial integrity in part by negatively regulating RhoA (Borikova et al., 2010; Richardson et al., 2013; Zheng et al., 2010). We and others characterized the roles of *C. elegans* GCK-1 and its co-factor Cerebral Cavernous Malformations – 3 (CCM-3; collectively, GCK-1/CCM-3) in maintaining structural integrity of the oogenic syncytial germline (Pal et al., 2017; Rehain-Bell et al., 2017). GCK-1/CCM-3 promote the stability of the intercellular bridges that connect developing oocytes with a shared cytoplasm by limiting the abundance of proteins that promote contractility (including anillin and NMM-II (NMY-2)) (Pal et al., 2017; Rehain-Bell et al., 2017). We proposed that GCK-1/CCM-3 suppress anillin and NMY-2 localization by inhibiting RhoA, as their vertebrate homologs are known to do (Rehain-Bell et al., 2017; Richardson et al., 2013).

The identification of novel anillin-interacting proteins that limit contractility fit logically with their localization to stable intercellular bridges. However, we and others noted that GCK-1/CCM-3 also enrich on the dynamic, contractile cytokinetic ring in the *C. elegans* zygote (Pal et al., 2017; Rehain-Bell et al., 2017). Here, we investigated the regulation of contractility in the *C. elegans* zygote by GCK-1/CCM-3. We found that on the contractile ring, GCK-1/CCM-3 also limit the abundance of "contractility" proteins and suppress contractility during cytokinesis and polarization of the zygote. GCK-1/CCM-3 localize to the cytokinetic ring downstream of the master regulator RhoA (and of anillin), but also influence the abundance of active RhoA. Therefore, we conclude that GCK-1/CCM-3 are novel components of negative feedback in the cytokinetic ring. These findings advance the growing body of work showing that contractile networks in cells are not only activated by positive regulation, but also contain structural "brakes" and regulatory time-delayed negative feedback important for turnover and dynamics (Bement et al., 2015; Bischof et al., 2017;

Dorn et al., 2016; Goryachev et al., 2016; Khaliullin et al., 2018; Michaux et al., 2018; Nishikawa et al., 2017).

## Results

*GCK-1 and CCM-3 regulate each other's stability and cortical targeting*

*C. elegans* GCK-1 and CCM-3 are known to interact, and their mammalian homologs form a heterodimer (Ceccarelli et al., 2011; Lant et al., 2015; Xu et al., 2013; Zhang et al., 2013). The domains that allow for heterodimerization of GCK III subfamily members and CCM3 are conserved in *C. elegans* GCK-1 and CCM-3 indicating that these proteins heterodimerize as well (Ceccarelli et al., 2011). However, the dynamics of GCK-1/CCM-3 localization and their interdependence during cytokinesis were unknown. We followed the anaphase localization of fluorescently-tagged GCK-1 and CCM-3 expressed under the control of their own promoters (Pal et al., 2017; Rehain-Bell et al., 2017). Both are present in the cytoplasm and enrich in the cytokinetic ring during anaphase (Figure 1A and B). We then depleted GCK-1 or CCM-3 by RNAi to test the requirement of each for localization of the other to the cytokinetic ring. Levels of GCK-1 or CCM-3 in the cytokinetic ring were significantly reduced following depletion of CCM-3 or GCK-1, respectively (Figure 1A, A', B, B'). These results demonstrate that GCK-1 and CCM-3 are interdependent for their enrichment on the cytokinetic ring and support the idea that they act as a complex during cytokinesis.

We next tested whether GCK-1 and CCM-3 affect each other's localization to the cytokinetic furrow via active recruitment or protein stabilization. To do so, we assessed the abundance of cytoplasmic GCK-1 or CCM-3 following depletion of the other (Figure 1C and C'). CCM-3 depletion did not significantly affect the cytoplasmic levels of GCK-1::GFP (Figure 1C).

Thus, we concluded that CCM-3 is not required for GCK-1 protein stability. Depletion of GCK-1, however, significantly decreased cytoplasmic levels of CCM-3::mNeonGreen (Figure 1C') suggesting that GCK-1 is required for CCM-3 stability. Consistently, we found that cytokinetic ring enrichment, the ratio of cytokinetic ring and cytoplasmic protein levels, of CCM-3::mNeonGreen increased slightly (~20%) following GCK-1 depletion compared to control, indicating approximately equal reduction of both the ring and cytoplasmic protein pools and little effect on ring targeting (Figure 1D'). Conversely, GCK-1::GFP enrichment on the cytokinetic ring relative to the cytoplasm was significantly decreased (~60% decrease) following CCM-3 depletion (Figure 1D). Together these results suggest that CCM-3 targets GCK-1 to the cytokinetic ring, while GCK-1 promotes CCM-3 ring localization at least partly by regulating CCM-3 protein stability.

*GCK-1 and CCM-3 localize downstream of RhoA*

RhoA is the master regulator necessary for recruitment and activation of cytokinetic ring components in animal cells (Basant and Glotzer, 2018; Jordan and Canman, 2012; Piekny et al., 2005). To test whether GCK-1/CCM-3 localize downstream of RhoA, we performed time-lapse imaging of GCK-1::GFP and CCM-3::mNeonGreen on the cell cortex during anaphase. Shortly following anaphase onset in control cells, both GCK-1 and CCM-3 localize to large cortical foci predominantly in the anterior half of the embryo and become enriched at the cell equator coinciding with the onset of cytokinesis (Figure 2A, Supplemental Figure 2 and data not shown). This localization pattern mirrors that of many known cytokinetic ring components such as active RhoA, anillin (ANI-1) and NMY-2 (Maddox et al., 2005; Maddox et al., 2007; Motegi et al., 2006; Schonegg et al., 2007; Velarde et al., 2007; Werner et al., 2007). In fact, GCK-1 and CCM-3

colocalized with NMY-2 during anaphase (Figure 2A, Supplemental movie 1 and data not shown). When the levels of active RhoA were reduced by partially depleting its main activator during cytokinesis the Rho GEF ECT-2 by RNAi, the levels of cortical GCK-1 at the cell equator during anaphase were significantly reduced (Figure 2B and C and Supplemental movie 2). We concluded that GCK-1/CCM-3 depend on active RhoA for recruitment to the cytokinetic ring.

RhoA effector proteins including Diaphanous-family formins, Rho-kinase, and anillin bind RhoA-GTP directly and independently, whereas downstream factors such as F-actin, NMY-2, and septins depend on these effectors (Heasman and Ridley, 2008; Piekny et al., 2005; Piekny and Maddox, 2010). To determine if GCK-1 localization is dependent on other cytokinetic ring components, we depleted ANI-1 or NMY-2 by RNAi and assessed GCK-1 levels in the cytokinetic ring. Depletion of ANI-1, but not NMY-2, caused a significant reduction in GCK-1 on the cell equator (Figure 2B, D and E and Supplemental movies 3 and 4). Taken together, these results demonstrate that GCK-1 and CCM-3 are recruited to the cytokinetic ring in a manner dependent on active RhoA and anillin but not NMY-2.

*GCK-1 and CCM-3 negatively regulate cytokinesis by limiting the amount of NMY-2 and anillin in the cytokinetic ring*

We previously found that GCK-1/CCM-3 attenuate NMM-II recruitment and ring stability in the syncytial germline (Rehain-Bell et al., 2017). To determine if GCK-1/CCM-3 play an analogous role during cytokinesis, we measured furrow ingression kinetics in embryos depleted of either GCK-1 or CCM-3. Thorough depletion of GCK-1 or CCM-3 leads to severe germline defects preventing the formation of normal embryos (Green et al., 2011; Maeda et al., 2001; Pal et al., 2017; Rehain-Bell et al., 2017); thus, here we studied the effect of partial CCM-3/GCK-1

depletion. Under these conditions, cytokinetic furrows ingressed to completion in all zygotes observed, suggesting that GCK-1/CCM-3 are not essential for completion of cytokinesis in the *C. elegans* zygote. However, we cannot exclude the possibility that thorough loss of function would lead to cytokinesis failure. Instead, embryos partially depleted of GCK-1/CCM-3 complete cytokinesis significantly faster than controls (Figure 3), suggesting that these novel ring components attenuate ring constriction.

To determine how GCK-1/CCM-3 affect cytokinetic ring ingression kinetics, we examined whether they are required for recruitment of cytokinetic ring components to the cell equator. The levels of both NMY-2 and anillin at the cell equator were significantly increased following GCK-1 or CCM-3 depletion (Figure 4A and B). This result suggests that GCK-1 and CCM-3 attenuate ingression speed by limiting the amount of proteins that drive contractility in the cytokinetic ring.

Vertebrate homologues of GCK-1 and CCM-3 negatively regulate RhoA activity (Borikova et al., 2010; Hwang and Pallas, 2014; Louvi et al., 2014; Richardson et al., 2013; Zheng et al., 2010). Therefore, we next tested whether *C. elegans* GCK-1/CCM-3 attenuate cytokinesis kinetics by negatively regulating RhoA activity. To do so, we generated a fluorescently-tagged Rho-kinase (LET-502), a well-characterized RhoA effector (Matsui et al., 1996), expressed from its endogenous locus to employ as a biosensor for RhoA activity. To characterize this probe, we experimentally increased or decreased RhoA activity by depleting its inactivator RhoGAP RGA-3/4 or activator RhoGEF ECT-2, respectively. Recruitment of Rho-kinase to the cell equator increased following RGA-3/4 depletion and decreased following ECT-2 depletion, thus correlating with the presumed abundance of active RhoA (Figure 4C and E and Supplemental movies 5-7). We then tested how depletion of GCK-1/CCM-3 altered active RhoA in the cell equator as

evidenced by the Rho-kinase probe. The abundance of equatorial Rho-kinase was significantly increased following GCK-1 or CCM-3 depletion, when compared to controls (Figure 4F).

Taken together, these results demonstrate that GCK-1/CCM-3 negatively regulate the kinetics of cytokinetic ring ingression, likely by limiting the amount of anillin and NMY-2 at the cell equator, which in turn is likely due to inhibiting RhoA.

*GCK-1 and CCM-3 negatively regulate cortical contractility during polarization*

The actomyosin cytoskeleton drives not only cytokinesis but a myriad of cellular events. For example, prior to the first mitotic division of the *C. elegans* zygote, a highly contractile actomyosin network spans the embryonic cortex and becomes progressively polarized to the embryo anterior. This reorganization of the cortical actomyosin network drives establishment of anterior-posterior polarity in a process known as polarization. During polarization a transient feature called the pseudocleavage furrow ingresses at the boundary of the highly contractile anterior and the more compliant posterior cortex, and regresses. The position and regulation of the pseudocleavage furrow are distinct from those of the cytokinetic furrow that ingresses about 10 minutes later (Cowan and Hyman, 2007; Werner and Glotzer, 2008); Figure 5A). To test whether GCK-1/CCM-3 regulate contractility only in cytokinesis or more generally, we investigated the roles of GCK-1/CCM-3 during *C. elegans* zygote polarization. We first observed that GCK-1/CCM-3 enrich in cortical patches during polarization, co-localizing with other contractile components such as NMY-2 and anillin, suggesting a role for GCK-1/CCM-3 contractility outside of cytokinesis (Figure 5B, Supplemental movie 8 and data not shown).

To test whether GCK-1/CCM-3 affect contractility during polarization, we depleted either CCM-3 or GCK-1 by RNAi and measured the depth and regression timing of the pseudocleavage

furrow, both of which reflect contractility during polarization (Reymann et al., 2016; Schmutz et al., 2007; Schonegg et al., 2007; Tse et al., 2012). The persistence of the pseudocleavage furrow was significantly increased in zygotes depleted of either CCM-3 or GCK-1 (Figure 5C and D and Supplemental movie 8). To control for possible defects in cell cycle progression, we also measured the time from pronuclear meeting to anaphase onset and found no statistically significant difference among control and embryos depleted of GCK-1 or CCM-3 indicating that cell cycle timing is not affected (Supplemental Figure 5A). Similarly, the maximal depth of pseudocleavage furrow as a percentage of embryo width was significantly increased following GCK-1 or CCM-3 depletion, when compared to controls (Figure 5C,E). An additional measure of cortical contractility during polarization is the size of the anterior polarity domain (Schonegg et al., 2007; Tse et al., 2012). The size of the anterior polarity domain, defined by localization of the anterior PAR protein PAR-6, was significantly reduced in embryos depleted of GCK-1 or CCM-3 when compared to controls (Figure 5F). This was not due to defects in polarity establishment or maintenance following depletion of CCM-3 or GCK-1, since these perturbations did not affect asymmetric spindle positioning or the extent of asymmetric enrichment of anterior PAR proteins (Figure S5, B-C''). Furthermore, GCK-1 and CCM-3 anterior localization during anaphase depended on PARs (Figure S4D, D', E, E') demonstrating that GCK-1 and CCM-3 localize downstream of PAR-driven polarity. Taken together these findings support the idea that GCK-1 and CCM-3 negatively regulate cortical contractility during polarization, in addition to cytokinesis and germline intercellular bridges.

*GCK-1/CCM-3 negatively regulate contractility by promoting negative feedback regulation of pulsed contractions.*

The actomyosin cortex that becomes polarized prior to the first mitotic division of the *C. elegans* zygote exhibits pulsed contractions such that regions of cortex stochastically undergo cycles of quiescence, activation, contraction, and finally relaxion and disassembly. This behavior has been increasingly used to study feedback loops in the regulation of contractility. During pulsed contractility, active RhoA recruits not only the actomyosin cytoskeleton, but also negative regulators of contractility, which in turn complete a time delayed negative feedback loop (Michaux et al., 2018; Naganathan et al., 2018; Nishikawa et al., 2017; Reymann et al., 2016). GCK-1/CCM-3 are implicated in negatively regulating RhoA (Borikova et al., 2010; Louvi et al., 2014; Zheng et al., 2010) and Figure 5G), but it is unknown whether they participate in time-delayed negative feedback.

To test whether GCK-1/CCM-3 regulate negative feedback during pulsed contractility, we first examined the timing of GCK-1 localization relative to contractile pulses. It has previously been shown that localization of active RhoA precedes the localization of NMY-2, Anillin and RGA-3 all of which localize concurrently (Michaux et al., 2018). We imaged cells co-expressing GFP-tagged GCK-1 and RFP-tagged NMY-2 with high temporal resolution and tracked cortical patches during polarization to determine the kinetics of GCK-1 localization relative to the accumulation of NMY-2. The maximal level of GCK-1 in cortical patches occurred approximately 3.5 seconds after that of NMY-2, consistent with a role in time-delayed negative feedback regulation of contractility (Figure 6A-D and Supplemental movie 9).

The established roles of GCK-1/CCM-3 in limiting RhoA activity and actomyosin contractility (Borikova et al., 2010; Louvi et al., 2014; Rehain-Bell et al., 2017; Zheng et al., 2010) and Figure 5G), together with their localization dependence on active RhoA and anillin, and delayed recruitment with respect to NMY-2, suggested that GCK-1/CCM-3 are not only upstream

but also downstream of cortical contractility, and thus contribute to a time-delayed negative feedback loop. This hypothesis makes the prediction that depleting GCK-1/CCM-3 would alter the kinetics of cortical pulses. Specifically, if GCK-1/CCM-3 suppressed RhoA activity upstream of pulsed activation, their depletion might prolong pulses. We therefore quantified the duration, change in intensity, and size of patches of active RhoA during pulsed contractility and found that neither duration nor change in intensity were significantly affected by GCK-1/CCM-3 depletion (Figure 6E). In fact, pulses intensified, compacted and dispersed with slightly, though not statistically significantly, faster kinetics than controls (Figure 6E and Supplemental Figure 6A-C). While the relative change in active RhoA was not different between GCK-1-depleted and control cells, RhoA probe intensity was uniformly higher throughout the entire pulse focus in GCK-1-depleted cells, compared to control cells (Figure 6E) leading to a small but significant increase in initial patch diameter (Figure 6F). These results suggest that GCK-1/CCM-3 modulate pulsed contractility by suppressing baseline RhoA activity.

In sum, our findings establish GCK-1/CCM-3 as novel negative regulators of actomyosin contractility during cytokinesis and other mitotic events.

## Discussion

Cytokinesis has been intensively studied for over a century, and novel cytokinetic ring proteins seldomly emerge. Here, we have characterized two recently identified cytokinetic ring proteins and their roles in regulating actomyosin contractility during cytokinesis. We found that GCK-1/CCM-3 are recruited downstream of active RhoA and the scaffold protein anillin, suggesting they are indirect RhoA effectors. However, we also found that GCK-1/CCM-3 limit Rho activity and actomyosin contractility during pulsed contractility, polarization, and cytokinesis

(Figure 5G), in agreement with what we and others have shown for the stable actomyosin cortex of the *C. elegans* syncytial germline (Pal et al., 2017; Priti et al., 2018; Rehain-Bell et al., 2017) Therefore, GCK-1/CCM-3 appear to contribute to a regulatory negative feedback loop acting on the RhoA-regulated actomyosin cytoskeleton.

We report that RhoA activity is required for equatorial enrichment of GCK-1/CCM-3. Several observations suggest that this is mediated by anillin (ANI-1): depletion of anillin prevents GCK-1/CCM-3 equatorial enrichment (Figure 2B and D), anillin recruitment is downstream of active RhoA (Hickson and O'Farrell, 2008; Piekny and Glotzer, 2008; Piekny and Maddox, 2010; Straight et al., 2003), and GCK-1 co-immunoprecipitates with ANI-1 (Rehain-Bell et al., 2017). Anillin is a large multi-domain scaffold protein with many binding partners and putative roles in cytokinesis (Piekny and Maddox, 2010). It is possible that some of the effects of anillin depletion during cytokinesis relate to the decreased GCK-1/CCM-3 recruitment. In fact, partial depletion of anillin increases maximal ingression speed during cytokinesis (Descovich et al., 2018) similar to what we observe for embryos depleted of GCK-1/CCM-3 (Figure 3A-C). While it was originally suggested that the increase in ingression speed following partial anillin depletions is due to a reduction in cytoskeletal crosslinking, our new results suggest that this effect may also be partly explained by loss of GCK-1/CCM-3.

Localization of GCK-1/CCM-3 to the cell equator during cytokinesis or cortical patches during pulsed contractions depends on active RhoA, leading us to conclude that the localization of these novel ring components is downstream of RhoA. However, our findings that GCK-1/CCM-3 depletion increased levels of active RhoA and contractility suggest that GCK-1/CCM-3 are upstream of, and negatively regulate, RhoA activation and actomyosin contractility (Figure 6G), consistent with previous work. Together, these findings suggest that GCK-1/CCM-3 participate in

a negative feed-back loop to regulate RhoA activity. The delay of GCK-1/CCM-3 localization to pulsed contractile cortical patches with respect to NMY-2 recruitment further supported this idea. However, our measurements of patch intensity, compaction and dissolution were inconsistent with the hypothesis that GCK-1/CCM-3 directly regulate the negative feedback loop driving pulsed contractions. Instead it appears that GCK-1/CCM-3 limits the amount of baseline RhoA activity in cortical patches at least partly by limiting the initial size of cortical patches (Figure 6 E, F). Higher baseline RhoA activity is expected to push a system of excitability and waves of pulsed contractility towards stable RhoA activation (Goryachev et al., 2016). We therefore predict that thorough loss of GCK-1/CCM-3, especially in combination with other RhoA activity gain-of-function perturbations, could cause constitutive cortical contractility and reduce the responsiveness of the cortex to spatial cues from the spindle.

Thorough depletion of GCK-1/CCM-3 leads to severe germline defects and precludes the formation of normal embryos. Therefore, we were unable to test the effects of thorough GCK-1/CCM-3 loss of function. Others reported cytokinetic furrow regression in a small subset of embryos, and polarity defects, following CCM-3 depletion (Pal et al., 2017). Our findings suggest that GCK-1/CCM-3 are downstream of PAR protein-based polarity and partial loss of GCK-1/CCM-3 does not prevent completion of cytokinesis. These differences could be explained by the extent of GCK-1/CCM-3 depletion, or the published cytokinesis failure and polarity defects could be secondary to defects in oocyte formation. Conditional alleles of GCK-1/CCM-3 would help reconcile these differences in the future. Such conditional alleles could also be used to test whether thorough loss of GCK-1/CCM-3 is sufficient to stably activate RhoA, as discussed above.

Another open question is the mechanism of RhoA inhibition by GCK-1/CCM-3. One potential mediator is the RhoGAP RGA-3/4, the central negative regulator of RhoA activity during

both polarization and cytokinesis, but depletion of RGA-3/4 leads to cellular phenotypes significantly different from those observed when GCK-1/CCM-3 are depleted (Schmutz et al., 2007; Schonegg et al., 2007). Another possible target is the ezrin, radixin, moesin (ERM) protein family, since studies with zebrafish and human cell culture suggest that phosphorylation of moesin by GCK-1 leads to reduction in RhoA activity (Zheng et al., 2010). In the future it would be interesting to test whether the only ERM family member in *C. elegans,* ERM-1, is a target of GCK-1 (the phosphorylation site is conserved between vertebrate moesin and ERM-1), and whether ERM-1 phosphorylation is involved in suppressing RhoA activity.

Taken together, our observations support the growing consensus that negative feedback regulation is important for the regulation of the cortical actomyosin cytoskeleton generally, and in cytokinesis in particular, and that GCK-1 and CCM-3 are important contributors to this negative feedback regulation.

## Materials and Methods

### C. elegans *strains and culture*

Worm strains (Table 1) were maintained using standard procedures at 20°C(Brenner, 1974). CRISPR knock-in of GFP at the N-terminus of LET-502 was carried out using an asymmetric repair template (0.5 kb of LET-502 promoter- GFP and 1.5 kb after LET-502 start site, injected at concentration of 20 ng/µl) and single worm PCR detection. sgRNA targeting the 5' end of LET-502 was cloned into pDD162 (Dickinson et al., 2013) and the plasmid (containing Cas9) was injected at concentration of 50 ng/ul.

**Table 1: Strains**

| Strain | Genotype | Publication |
|---|---|---|

| | | |
|---|---|---|
| EM328 | *let-502(mc74[GFP::let-502}I; (zuIs151 [nmy-2::NMY-2-mRFP; unc-119(+)]* | this study |
| LP162 | *cp13[nmy-2::gfp + LoxP]) I.* | *(Dickinson et al., 2013)* |
| MDX33 | *cpIs45[Pmex-5::mNeonGreen::PLCδ-PH::tbb-2 3'UTR + unc-119(+)] II; unc-119(ed3) III; his-72 cp10 [his-72::gfp+LoxP unc-119(+) LoxP] III* | this study |
| MDX38 | *ccm-3(mon9[ccm-3::mNeonGreen^Flag]) II* | *(Rehain-Bell et al., 2017)* |
| MDX40 | *nmy-2(cp52[nmy-2::mkate2 + LoxP unc-119(+) LoxP]) I; unc-119(ed3) III; ani-1(mon7[mNeonGreen^3xFlag::ani-1]) III* | *(Rehain-Bell et al., 2017)* |
| MDX69 | *par-6(cp70[par-6::mKate^3xFlag]) I; ccm-3(mon9[ccm-3::mNeonGreen^Flag]) II* | this study |
| MDX74 | *par-6(cp70[par-6::mKate^3xFlag]) I; gck-1(onIs15[GFP::3xFlag::gck-1])III* | this study |
| MDX77 | *nmy-2(cp52[nmy-2::mkate2 + LoxP unc-119(+) LoxP]) I; unc-119(ed3) III; gck-1(onIs15[GFP::3xFlag::gck-1])III* | this study |
| WD478 | *gck-1(onIs15[GFP::3xFlag::gck-1])III* | *(Pal et al., 2017)* |

*RNA-mediated interference*

Depletions were conducted by feeding worms bacteria, from the Ahringer collection, expressing double-strand RNA (dsRNA) as described in for 20-24 hours in all conditions (Kamath and Ahringer, 2003; Kamath et al., 2003).

C. elegans *embryo sample prep and live imaging conditions*

Embryos were dissected from gravid hermaphrodites and mounted on 2% agar pads except for Figures 3C and Figure 4A and B for which embryos were mounted as inverted hanging drops. Images for Figures 1, 3A-B and D, 5C-F and Supplemental Figures 2 and 5 were acquired with a CoolSnap Hq camera (Photometrics) mounted on a DeltaVision Image Restoration System (GE) with a 60x/1.42 NA Plan Apochromat objective. For Figure 1 and Supplemental Figure 2, we acquired z-stacks with 1μm spacing through the entire embryo every 20 seconds and every 15

seconds for Figure 5C-E. Data for Figure 5 Supplement were gathered by taking single images at the midplane of the embryo every 60 seconds.

Data for Figures 2, 3C, 4, 5B, 6 and Figure 6 Supplement were acquired on a Nikon A1R microscope body with a 60X 1.27 NA Nikon Water Immersion Objective (Figure 3C and Figure 4 A and B) or 60x 1.41 NA Nikon Oil Immersion Objective (Figures 2, 4C-F, 5B, 6 and Figure 6 Supplement) with a GaASP PMT detector using NIS-elements. For Figure 3C and 4A and B 40 Z-stacks with 1μm spacing through the entire embryo were acquired every 2.7 seconds using the resonance scanner. All other data acquired on the A1R were from single Z-sections at the embryonic cortex with a sampling frequency of 1 second using the Galvano point scanner.

*Segmentation and analysis of fluorescence in the cytokinetic ring*

For Figures 1A-B and 3C the ImageJ based software FIJI was used to analyze z-stacks of the full embryo [31]. First, the cytokinetic ring was isolated. Then, an end-on reconstruction was generated. The signal in this end-on reconstruction was automatically segmented utilizing the Weka-segmentation plugin. In MATLAB, an ellipsoid was fitted to the segmented signal at each time point giving a measurement of ring perimeter. Fluorescence intensity on the ring at each time-point was measured from sum-projections of background corrected images where the signal was identified by Weka-segmentation.

For all other quantifications of equatorial fluorescence levels single cortical planes (Figures 2C-E, 4D-F) or sum intensity projection of z-stacks (Figure 4A and B-E) were analyzed in FIJI by preforming a line scan with a width of 5um centered around the ingressing furrow. Mean intensity values were calculated and background adjusted using custom MATLAB scripts by subtracting

the mean fluorescence intensity of a 5 μm by 5 μm region in the posterior half of the embryo from the mean intensity data at each time point.

*Analysis of cytoplasmic protein levels and cytokinetic ring enrichment*

Average fluorescence intensity in the cytoplasm was measured using FIJI from background corrected images. Enrichment on the ring at ~50% closure was calculated by dividing ring average fluorescence by cytoplasmic average fluorescence at the same time point (Figure 1C-D').

*Line scan analysis and calculation of anterior enrichment.*

Line scan analysis was performed using FIJI. Lines were drawn along the cortex from the anterior to posterior end of the embryo. The Graphpad software PRISM was then used to fit a sigmoidal line to the data and to calculate the LogIC50. The LogIC50 marks the inflection point where anterior enrichment ends. Anterior enrichment was calculated by determining the ratio of average fluorescence intensity of the most anterior 25% of the cortex to the average fluorescence intensity of the most posterior 25% of the cortex (Figure 2 and 5 Supplements).

*Analysis of pseudocleavage furrow depth and persistence*

In the MDX33 strain, which expresses both a membrane and DNA marker, we used FIJI to measure the distance between the two ends of the pseudocleavage furrow at the point of maximal ingression. This number was then subtracted from the total embryo width to determine the depth of the pseudocleavage furrow. To normalize between conditions, we converted the pseudocleavage depth to a percentage of embryo width (Figure 5E). To measure the persistence of the

pseudocleavage furrow the time from full regression of the pseudocleavage furrow to pronuclear meeting was calculated (Figure 5D).

*Analysis of total ingression time*

We imaged cytokinesis in the strain MDX33, which expresses both a membrane and DNA marker, with 2.7 second time resolution and calculated the time from initiation defined as the first indentation of the membrane following anaphase onset, to ~100% closure of the cytokinetic ring, defined as the point when the cytokinetic ring did not decrease in size in the next two time points (Figure 3B).

*Tracking and analyzing cortical foci*

Cortical foci during polarization were identified and tracked using FIJI plugin Trackmate. For this purpose, images were normalized and thresholded in ImageJ to create a binary mask for each time point. The stack of binary masks was combined with the raw data into a hyperstack that was used in trackmate. Foci were tracked using the binary mask and values within the tracked areas on the raw data were used for quantitative analysis. We used the Trackmate LoG detector with an estimated foci diameter of 3 μm to detect foci and the simple LAP tracer function with maximum linking distance of 2 μm, a max Gap closing distance of 2 μm and a Gap closing max frame gap of 2 to track foci over time. Processing and analysis of foci properties determined using trackmate was performed using custom scripts in MATLAB.

*Figures and statistical analysis*

Figures were generated using Microsoft Excel, MATLAB or GraphPad PRISM software, Statistical significance was determine using a 2-tailed Student's t-test. Assumptions for normality and equal variance were met for all data analyzed. A p-value of less than 0.05 from a two-tailed t-test was considered significant. Results of the statistical analysis are shown in all figures. All error bars represent standard error unless stated otherwise in the figure legends. Sample size (n) and p-values are given on each figure panel or in the figure legends.

## Figure & Movie Legends

**Figure 1. Mutual regulation of GCK-1 and CCM-3 enrichment on the cytokinetic ring**.

A) Representative single plane images of control and *gck-1(RNAi)* embryos expressing CCM-3::mNeonGreen. B) Representative single plane images of control and *ccm-3(RNAi)* embryos expressing GCK-1::GFP. A' and B') Quantitation of average fluorescence intensity per micron relative to the perimeter of the cytokinetic ring in control (n=7 embryos) and depleted (n= 9 or 6 embryos (GCK-1 or CCM-3 depleted, respectively)) conditions. C and C') Cytoplasmic levels of GCK-1::GFP (C) and CCM-3::mNeonGreen (C') in control and depleted cells. D and D') Enrichment of GCK-1::GFP (D) and CCM-3::mNeonGreen (D') on the cytokinetic ring relative to the cytoplasm in control and depleted cells. Scale bars = 10 μm in all images in all figures. Error bars = SE in all figures unless otherwise indicated.

**Figure 2. GCK-1 localization is dependent on active RhoA and anillin but not NMMII.**

A) Representative images of GCK-1::GFP and NMY-2:mKate localization during anaphase. B) Representative images of embryos expressing both GCK-1:GFP and NMY-2::mKate in control,

*ect-2(RNAi), ani-1(RNAi)* and *nmy-2(RNAi)* embryos 60 seconds after anaphase onset. C-E) Background-adjusted equatorial GCK-1:GFP levels normalized to that at anaphase onset in control, *ect-2(RNAi)* (C), *ani-1(RNAi)* (D) and *nmy-2(RNAi)* (E) embryos (n=6 for all conditions).

**Figure 2 Supplement. GCK-1 and CCM-3 are polarized to the zygote anterior.**

A) Representative midplane image of GCK-1::GFP localization at cytokinesis initiation. A: embryo anterior; P: posterior. A') Representative line scans of cortical GCK-1::GFP average fluorescence from the anterior (A) to posterior (P) and sigmoidal fit (LogIC50 = 63.43. B) Representative midplane image of CCM-3::mNeonGreen localization at cytokinesis initiation. B') Representative line scans of cortical CCM-3::mNeonGreen average fluorescence from the anterior (A) to posterior (P) and sigmoidal fit (LogIC50 = 61.98). C) Inflection point (end of the anterior enrichment region; LogIC50) of sigmoidal lines fit to line scan analysis of cortical GCK-1::GFP (n=6 embryos) and CCM-3::mNeonGreen (n=21 embryos) from anterior to posterior.

**Figure 3. Depletion of GCK-1 or CCM-3 causes increased cytokinetic ingression speed.**

A) Representative montage of HIS:GFP and mNeonGreen::PH in the furrow region over time in control, *gck-1(RNAi)* and *ccm-3(RNAi)* embryos. Colored bars represent the timing of distinct phases of cytokinesis shown in the schematic below. Initiation: anaphase onset - onset of furrow ingression. Involution: onset of ingression - appearance of a doubled membrane. Furrowing: the appearance of doubled membrane - complete ring closure. B) Quantification of the duration of interval between furrowing onset and ring closure. C-D) Cytokinetic ring closure dynamics in control (n=9), *gck-1(RNAi)* (n=7) and *ccm-3(RNAi)* (n=6) embryos measured by following closure

dynamics (C) or subdividing cytokinesis timing into 3 distinct stages (D) using a strain expressing mNeonGreen::ANI-1 and NMY-2:mKate2. Error bars are standard deviation.

**Figure 4: GCK-1/CCM-3 limit the amount of equatorial anillin and NMM-II and suppress RhoA activity.**

A) Quantification of background-adjusted equatorial mNeonGreen::ANI-1 levels relative to equatorial levels 20 seconds prior to onset of furrow ingression in control (n=6), *gck-1(RNAi)* (n=9) *or ccm-3(RNAi)* (n=9) embryos. B) Quantification of background-adjusted equatorial NMY-2::GFP levels relative to equatorial levels 20 seconds prior to onset of furrow ingression in control (n=9), *gck-1(RNAi)* (n=10) and *ccm-3(RNAi)* (n=12) embryos. C) Representative images of endogenous GFP::LET-502 at onset of ingression in control, *ect-2(RNAi)* or *rga-3/4(RNAi)* embryos. D) Background-adjusted total equatorial GFP::LET-502 fluorescence levels in control embryos (n=7) and embryos with increased (*rga-3/4(RNAi)* (n=6)) or decreased (*ect-2(RNAi)* (n=6)) active RhoA levels. E) Relative increase in background adjusted total equatorial GFP::LET-502 fluorescence levels in control embryos and embryos with increased (*rga-3/4(RNAi)*) or decreased (*ect-2(RNAi)*) active RhoA levels. F) Quantification of background-adjusted equatorial GFP::LET-502 levels relative to equatorial levels 30 seconds prior to onset of furrow ingression in control (n=7), *gck-1(RNAi)* (n=10) and *ccm-3(RNAi)* (n=10) embryos.

**Figure 5. GCK-1 localizes to cortical patches during polarization and inhibits cortical contractility.**

A) Schematic representation cellular morphology and distribution of relevant protein complexes in the *C. elegans* zygote. B) Representative images of single plane cortical imaging of embryos

expressing GCK-1::GFP and NMY-2::mKate2. C) Representative fluorescent images of control, *gck-1(RNAi) and ccm-3(RNAi)* embryos expressing HIS::GFP and mNeonGreen::PH (Top) and corresponding DIC images (bottom). Left: maximal pseudocleavage furrow ingression depth; Right: at pronuclear meeting. D) Quantification of the time interval between pronuclear meeting and complete regression of the pseudocleavage furrow in control, *gck-1(RNAi) and ccm-3(RNAi)* embryos. (E) Quantification of maximal pseudocleavage ingression as a percentage of cell width in control, *gck-1(RNAi)* and *ccm-3(RNAi)* embryos. (F) Quantification of the size of the anterior PAR domain at metaphase in control, *gck-1(RNAi) and ccm-3(RNAi)* embryos expressing PAR-6::mKate2.

**Figure 5 Supplement. GCK-1/CCM-3 are downstream of polarity.**

A) Quantification of the time from onset of nuclear envelope breakdown (NEBD) to anaphase in embryos expressing HIS::GFP and mNeonGreen::PH under control, *gck-1(RNAi)* or *ccm-3(RNAi)* conditions. B) Schematics of anterior (red) and posterior (blue) cortical domains at metaphase in the *C. elegans* zygote, and of mutual antagonism between PAR complexes (at right). C) Representative single midplane images of PAR-6::mKate2 in control, *gck-1(RNAi)*, and *ccm-3(RNAi)* embryos. C', C") Quantification of the effect of *gck-1(RNAi)* and *ccm-3(RNAi)* on anterior enrichment of PAR-6::mKate2 cortical fluorescence (B') and spindle position (B"). n.s. = no significant difference. D) Representative single midplane images of CCM-3::GFP in control and *par-6(RNAi)* embryos. D') Quantification of anterior enrichment of CCM-3::GFP cortical fluorescence and spindle position in control and *par-6(RNAi)* conditions. E) Representative single midplane images of GCK-1::GFP in control and *par-6(RNAi)* embryos. E') Quantification of

anterior enrichment of GCK-1::GFP cortical fluorescence and spindle position in control and *par-6(RNAi)* embryos.

**Figure 6. GCK-1 localizes to cortical foci after NMM-II and limits RhoA activity on the cortex.**

A) Kymograph showing pulsed GCK-1::GFP and NMY-2::mKate2 localization during embryo polarization. B) Magnified view of GCK-1::GFP and NMY-2::mKate2 localization to a single focus. C) Mean accumulation profile of GCK-1::GFP and NMY-2:mKate2 in cortical patches D) Time delay in maximal GCK-1::GFP accumulation relative to NMY-2::mKate2 localization. Data points = individual foci, Error bars = SD. n=423 total patches from 8 embryos for C and D. E) Mean fluorescence intensity profile of GFP::LET-502 in cortical patches from control and *gck-1(RNAi)* embryos. F) Mean estimated diameter profiles of cortical patches based on GFP::LET-502 fluorescence. G) Summary diagram of relationship of GCK-1/CCM-3 to canonical cytokinetic contractility regulation network.

**Figure 6 Supplement. GCK-1 depletion does not change focus dynamics during pulsed contractility.**

(A) Width at half max of for all intensity measurements shown in Fig 5E of Rho Activity in individual foci in control and *gck-1(RNAi)* embryos. Width at half max measurements of RhoA activity increases (B) and decreases (C) in individual patches for control and *gck-1(RNAi)* embryos. Error bars = standard deviations.

**Supplemental movie 1.** Single cortical plane imaging of control embryos expressing GCK-1::GFP (left, green) and NMY-2::mKate (middle, red) during anaphase. Acquisition rate 1 frame per second for all Supplemental movies.

**Supplemental movie 2.** Single cortical plane imaging of embryos expressing GCK-1::GFP (left, green) and NMY-2::mKate (middle, red) during anaphase after ECT-2 depletion by RNAi.

**Supplemental movie 3.** Single cortical plane imaging of embryos expressing GCK-1::GFP (left, green) and NMY-2::mKate (middle, red) during anaphase after ANI-1 depletion by RNAi.

**Supplemental movie 4.** Single cortical plane imaging of embryos expressing GCK-1::GFP (left, green) and NMY-2::mKate (middle, red) during anaphase after NMY-2 depletion by RNAi.

**Supplemental movie 5.** Single cortical plane imaging of control embryos expressing GFP::LET-502.

**Supplemental movie 6.** Single cortical plane imaging of embryos expressing GFP::LET-502 (left, green) after ECT-2 depletion by RNAi.

**Supplemental movie 7.** Single cortical plane imaging of embryos expressing GFP::LET-502 (left, green) after RGA-3/4 depletion by RNAi.

**Supplemental movie 8.** Single cortical plane imaging of control embryos expressing GCK-1::GFP (left, green) and NMY2::mKate (middle, red) during polarization.

**Supplemental movie 9.** Overlay of single cortical plane imaging of control embryos expressing GCK-1::GFP (green) and NMY2::mKate (red) with tracked areas identified by ImageJ trackmate (purple) during polarization.

## Acknowledgements

We thank Edwin Munro, Dan Dickinson and Brent Derry for providing worm strains. Members of the Maddox labs especially Paul Maddox, Jenna Perry and Vincent Boudreau for critical reading and discussion of the manuscript. KRB was supported in part by a grant from the National Institute of General Medical Sciences under award 5T32 GM007092. This work was supported by European Research Council grant #294744 to ML, and GM102390 from the NIH and 1616661 from the NSF to ASM.

## References

Basant, A., and M. Glotzer. 2018. Spatiotemporal Regulation of RhoA during Cytokinesis. *Curr Biol*. 28:R570-R580.

Bement, W.M., M. Leda, A.M. Moe, A.M. Kita, M.E. Larson, A.E. Golding, C. Pfeuti, K.C. Su, A.L. Miller, A.B. Goryachev, and G. von Dassow. 2015. Activator-inhibitor coupling between Rho signalling and actin assembly makes the cell cortex an excitable medium. *Nat Cell Biol*. 17:1471-1483.

Bischof, J., C.A. Brand, K. Somogyi, I. Majer, S. Thome, M. Mori, U.S. Schwarz, and P. Lenart. 2017. A cdk1 gradient guides surface contraction waves in oocytes. *Nat Commun*. 8:849.

Borikova, A.L., C.F. Dibble, N. Sciaky, C.M. Welch, A.N. Abell, S. Bencharit, and G.L. Johnson. 2010. Rho kinase inhibition rescues the endothelial cell cerebral cavernous malformation phenotype. *J Biol Chem*. 285:11760-11764.

Brenner, S. 1974. The genetics of Caenorhabditis elegans. *Genetics*. 77:71-94.

Brugues, J., B. Maugis, J. Casademunt, P. Nassoy, F. Amblard, and P. Sens. 2010. Dynamical organization of the cytoskeletal cortex probed by micropipette aspiration. *Proc Natl Acad Sci U S A*. 107:15415-15420.

Ceccarelli, D.F., R.C. Laister, V.K. Mulligan, M.J. Kean, M. Goudreault, I.C. Scott, W.B. Derry, A. Chakrabartty, A.C. Gingras, and F. Sicheri. 2011. CCM3/PDCD10 heterodimerizes with germinal center kinase III (GCKIII) proteins using a mechanism analogous to CCM3 homodimerization. *J Biol Chem*. 286:25056-25064.

Cheffings, T.H., N.J. Burroughs, and M.K. Balasubramanian. 2016. Actomyosin Ring Formation and Tension Generation in Eukaryotic Cytokinesis. *Curr Biol*. 26:R719-R737.

Cowan, C.R., and A.A. Hyman. 2007. Acto-myosin reorganization and PAR polarity in C. elegans. *Development*. 134:1035-1043.

D'Avino, P.P. 2009. How to scaffold the contractile ring for a safe cytokinesis - lessons from Anillin-related proteins. *J Cell Sci*. 122:1071-1079.

D'Avino, P.P., M.G. Giansanti, and M. Petronczki. 2015. Cytokinesis in animal cells. *Cold Spring Harb Perspect Biol*. 7:a015834.

Descovich, C.P., D.B. Cortes, S. Ryan, J. Nash, L. Zhang, P.S. Maddox, F. Nedelec, and A.S. Maddox. 2018. Cross-linkers both drive and brake cytoskeletal remodeling and furrowing in cytokinesis. *Mol Biol Cell*. 29:622-631.

Dickinson, D.J., J.D. Ward, D.J. Reiner, and B. Goldstein. 2013. Engineering the Caenorhabditis elegans genome using Cas9-triggered homologous recombination. *Nat Methods*. 10:1028-1034.

Dorn, J.F., L. Zhang, T.-T. Phi, B. Lacroix, P.S. Maddox, J. Liu, and A.S. Maddox. 2016. A theoretical model of cytokinesis implicates feedback between membrane curvature and cytoskeletal organization in asymmetric cytokinetic furrowing. *Molecular Biology of the Cell*. 27:1286-1299.

Goryachev, A.B., M. Leda, A.L. Miller, G. von Dassow, and W.M. Bement. 2016. How to make a static cytokinetic furrow out of traveling excitable waves. *Small GTPases*. 7:65-70.

Green, R.A., H.L. Kao, A. Audhya, S. Arur, J.R. Mayers, H.N. Fridolfsson, M. Schulman, S. Schloissnig, S. Niessen, K. Laband, S. Wang, D.A. Starr, A.A. Hyman, T. Schedl, A. Desai, F. Piano, K.C. Gunsalus, and K. Oegema. 2011. A high-resolution C. elegans essential gene network based on phenotypic profiling of a complex tissue. *Cell*. 145:470-482.

Green, R.A., E. Paluch, and K. Oegema. 2012. Cytokinesis in Animal Cells. *Annu Rev Cell Dev Bi*. 28:29-+.

Heasman, S.J., and A.J. Ridley. 2008. Mammalian Rho GTPases: new insights into their functions from in vivo studies. *Nat Rev Mol Cell Biol*. 9:690-701.

Hickson, G.R., and P.H. O'Farrell. 2008. Rho-dependent control of anillin behavior during cytokinesis. *J Cell Biol*. 180:285-294.

Hwang, J., and D.C. Pallas. 2014. STRIPAK complexes: structure, biological function, and involvement in human diseases. *Int J Biochem Cell Biol*. 47:118-148.

Jordan, S.N., and J.C. Canman. 2012. Rho GTPases in animal cell cytokinesis: an occupation by the one percent. *Cytoskeleton (Hoboken)*. 69:919-930.

Kamath, R.S., and J. Ahringer. 2003. Genome-wide RNAi screening in Caenorhabditis elegans. *Methods*. 30:313-321.

Kamath, R.S., A.G. Fraser, Y. Dong, G. Poulin, R. Durbin, M. Gotta, A. Kanapin, N. Le Bot, S. Moreno, M. Sohrmann, D.P. Welchman, P. Zipperlen, and J. Ahringer. 2003. Systematic functional analysis of the Caenorhabditis elegans genome using RNAi. *Nature*. 421:231-237.

Khaliullin, R.N., R.A. Green, L.Z. Shi, J.S. Gomez-Cavazos, M.W. Berns, A. Desai, and K. Oegema. 2018. A positive-feedback-based mechanism for constriction rate acceleration during cytokinesis in Caenorhabditis elegans. *Elife*. 7.

Lacroix, B., and A.S. Maddox. 2012. Cytokinesis, ploidy and aneuploidy. *J Pathol*. 226:338-351.

Lant, B., B. Yu, M. Goudreault, D. Holmyard, J.D. Knight, P. Xu, L. Zhao, K. Chin, E. Wallace, M. Zhen, A.C. Gingras, and W.B. Derry. 2015. CCM-3/STRIPAK promotes seamless tube extension through endocytic recycling. *Nat Commun*. 6:6449.

Louvi, A., S. Nishimura, and M. Gunel. 2014. Ccm3, a gene associated with cerebral cavernous malformations, is required for neuronal migration. *Development*. 141:1404-1415.

Maddox, A.S., B. Habermann, A. Desai, and K. Oegema. 2005. Distinct roles for two C. elegans anillins in the gonad and early embryo. *Development*. 132:2837-2848.

Maddox, A.S., L. Lewellyn, A. Desai, and K. Oegema. 2007. Anillin and the septins promote asymmetric ingression of the cytokinetic furrow. *Dev Cell*. 12:827-835.

Maeda, I., Y. Kohara, M. Yamamoto, and A. Sugimoto. 2001. Large-scale analysis of gene function in Caenorhabditis elegans by high-throughput RNAi. *Curr Biol*. 11:171-176.

Matsui, T., M. Amano, T. Yamamoto, K. Chihara, M. Nakafuku, M. Ito, T. Nakano, K. Okawa, A. Iwamatsu, and K. Kaibuchi. 1996. Rho-associated kinase, a novel serine/threonine kinase, as a putative target for small GTP binding protein Rho. *EMBO J*. 15:2208-2216.

Michaux, J.B., F.B. Robin, W.M. McFadden, and E.M. Munro. 2018. Excitable RhoA dynamics drive pulsed contractions in the early C. elegans embryo. *J Cell Biol*. 217:4230-4252.

Motegi, F., N.V. Velarde, F. Piano, and A. Sugimoto. 2006. Two phases of astral microtubule activity during cytokinesis in C. elegans embryos. *Dev Cell*. 10:509-520.

Naganathan, S.R., S. Furthauer, J. Rodriguez, B.T. Fievet, F. Julicher, J. Ahringer, C.V. Cannistraci, and S.W. Grill. 2018. Morphogenetic degeneracies in the actomyosin cortex. *Elife*. 7.

Nishikawa, M., S.R. Naganathan, F. Julicher, and S.W. Grill. 2017. Controlling contractile instabilities in the actomyosin cortex. *Elife*. 6.

Pal, S., B. Lant, B. Yu, R. Tian, J. Tong, J.R. Krieger, M.F. Moran, A.C. Gingras, and W.B. Derry. 2017. CCM-3 Promotes C. elegans Germline Development by Regulating Vesicle Trafficking Cytokinesis and Polarity. *Curr Biol*. 27:868-876.

Piekny, A., M. Werner, and M. Glotzer. 2005. Cytokinesis: welcome to the Rho zone. *Trends Cell Biol*. 15:651-658.

Piekny, A.J., and M. Glotzer. 2008. Anillin is a scaffold protein that links RhoA, actin, and myosin during cytokinesis. *Curr Biol*. 18:30-36.

Piekny, A.J., and A.S. Maddox. 2010. The myriad roles of Anillin during cytokinesis. *Semin Cell Dev Biol*. 21:881-891.

Pollard, T.D., and B. O'Shaughnessy. 2019. Molecular Mechanism of Cytokinesis. *Annu Rev Biochem*.

Priti, A., H.T. Ong, Y. Toyama, A. Padmanabhan, S. Dasgupta, M. Krajnc, and R. Zaidel-Bar. 2018. Syncytial germline architecture is actively maintained by contraction of an internal actomyosin corset. *Nat Commun*. 9:4694.

Rehain-Bell, K., A. Love, M.E. Werner, I. MacLeod, J.R. Yates, 3rd, and A.S. Maddox. 2017. A Sterile 20 Family Kinase and Its Co-factor CCM-3 Regulate Contractile Ring Proteins on Germline Intercellular Bridges. *Curr Biol*. 27:860-867.

Reymann, A.C., F. Staniscia, A. Erzberger, G. Salbreux, and S.W. Grill. 2016. Cortical flow aligns actin filaments to form a furrow. *eLife*. 5:1-25.

Richardson, B.T., C.F. Dibble, A.L. Borikova, and G.L. Johnson. 2013. Cerebral cavernous malformation is a vascular disease associated with activated RhoA signaling. *Biol Chem*. 394:35-42.

Schmutz, C., J. Stevens, and A. Spang. 2007. Functions of the novel RhoGAP proteins RGA-3 and RGA-4 in the germ line and in the early embryo of C. elegans. *Development*. 134:3495-3505.

Schonegg, S., A.T. Constantinescu, C. Hoege, and A.A. Hyman. 2007. The Rho GTPase-activating proteins RGA-3 and RGA-4 are required to set the initial size of PAR domains in Caenorhabditis elegans one-cell embryos. *Proc Natl Acad Sci U S A*. 104:14976-14981.

Schouest, K.R., Y. Kurasawa, T. Furuta, N. Hisamoto, K. Matsumoto, and J.M. Schumacher. 2009. The germinal center kinase GCK-1 is a negative regulator of MAP kinase activation and apoptosis in the C. elegans germline. *PLoS One*. 4:e7450.

Straight, A.F., A. Cheung, J. Limouze, I. Chen, N.J. Westwood, J.R. Sellers, and T.J. Mitchison. 2003. Dissecting Temporal and Spatial Control of Cytokinesis with a Myosin II Inhibitor. *Science*. 299:1743-1748.

Tse, Y.C., M. Werner, K.M. Longhini, J.C. Labbe, B. Goldstein, and M. Glotzer. 2012. RhoA activation during polarization and cytokinesis of the early Caenorhabditis elegans embryo is differentially dependent on NOP-1 and CYK-4. *Mol Biol Cell*. 23:4020-4031.

Velarde, N., K.C. Gunsalus, and F. Piano. 2007. Diverse roles of actin in C. elegans early embryogenesis. *BMC Dev Biol*. 7:142.

Werner, M., and M. Glotzer. 2008. Control of cortical contractility during cytokinesis. *Biochem Soc Trans*. 36:371-377.

Werner, M., E. Munro, and M. Glotzer. 2007. Astral Signals Spatially Bias Cortical Myosin Recruitment to Break Symmetry and Promote Cytokinesis. *Current Biology*. 17:1286-1297.

Xu, X., X. Wang, Y. Zhang, D.C. Wang, and J. Ding. 2013. Structural basis for the unique heterodimeric assembly between cerebral cavernous malformation 3 and germinal center kinase III. *Structure*. 21:1059-1066.

Yin, H., Z. Shi, S. Jiao, C. Chen, W. Wang, M.I. Greene, and Z. Zhou. 2012. Germinal center kinases in immune regulation. *Cell Mol Immunol*. 9:439-445.

Zhang, M., L. Dong, Z. Shi, S. Jiao, Z. Zhang, W. Zhang, G. Liu, C. Chen, M. Feng, Q. Hao, W. Wang, M. Yin, Y. Zhao, L. Zhang, and Z. Zhou. 2013. Structural mechanism of CCM3 heterodimerization with GCKIII kinases. *Structure*. 21:680-688.

Zheng, X., C. Xu, A. Di Lorenzo, B. Kleaveland, Z. Zou, C. Seiler, M. Chen, L. Cheng, J. Xiao, J. He, M.A. Pack, W.C. Sessa, and M.L. Kahn. 2010. CCM3 signaling through sterile 20-like kinases plays an essential role during zebrafish cardiovascular development and cerebral cavernous malformations. *J Clin Invest*. 120:2795-2804.

Figure 1

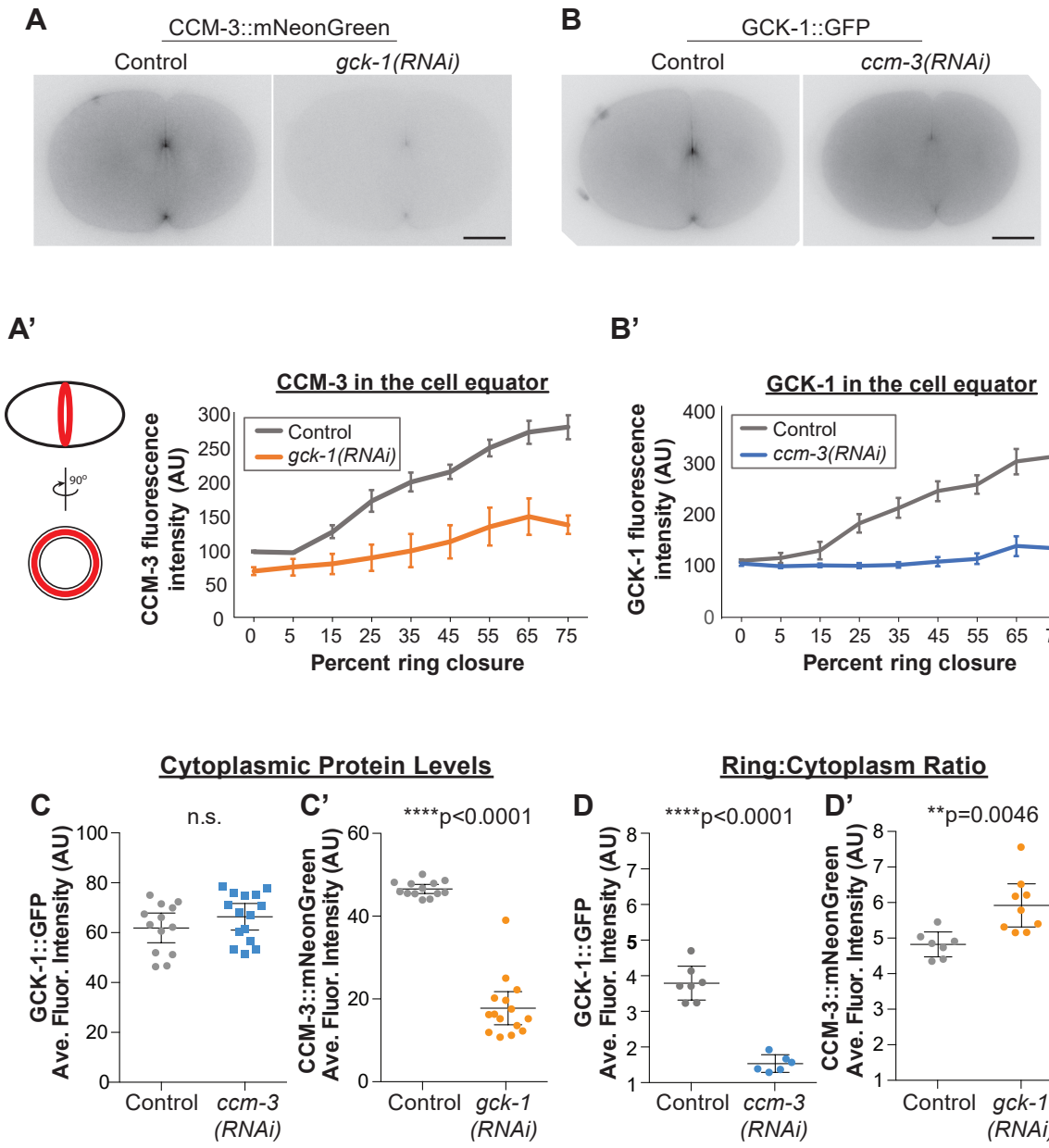

Figure 2

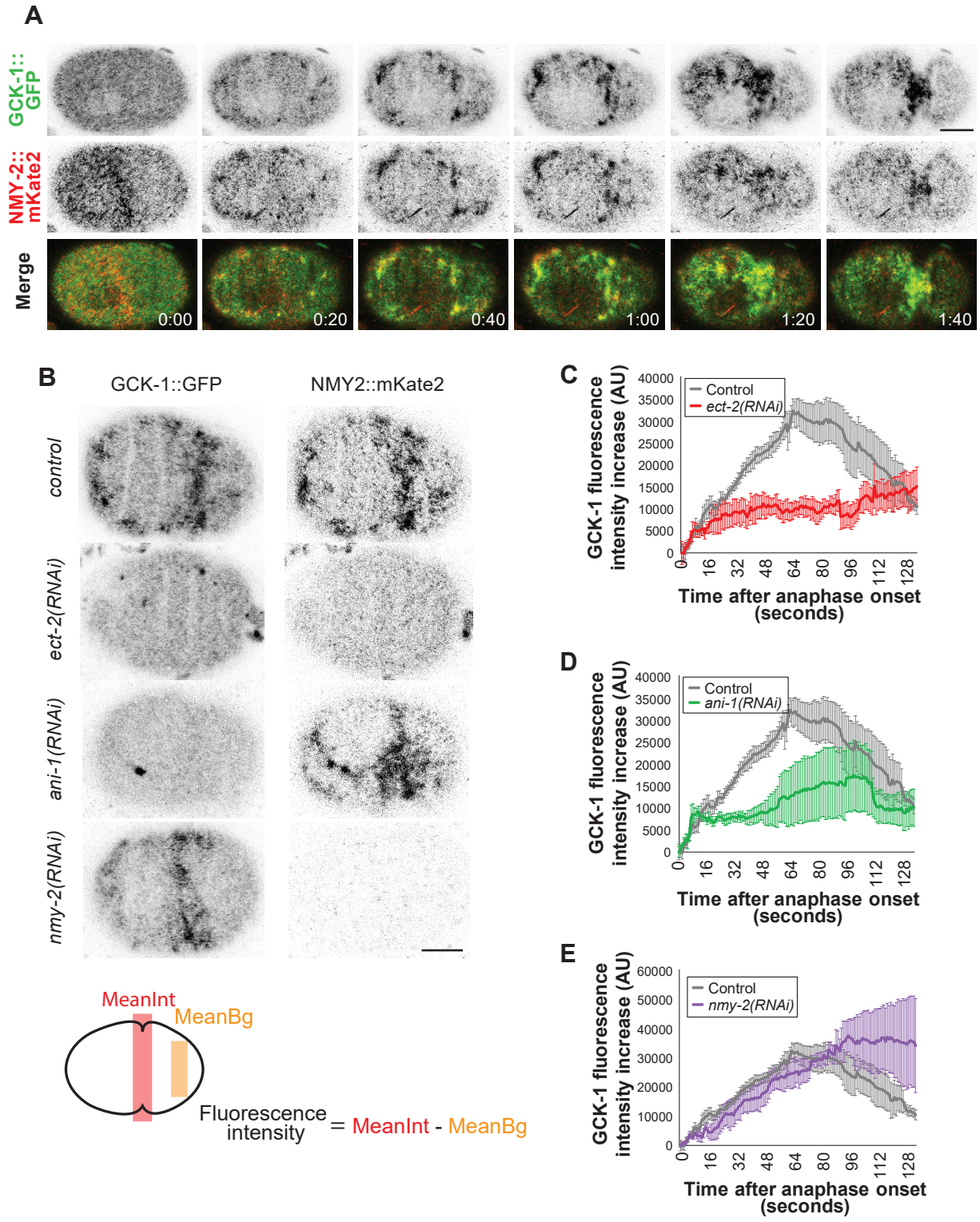

# Figure 2 Supplement

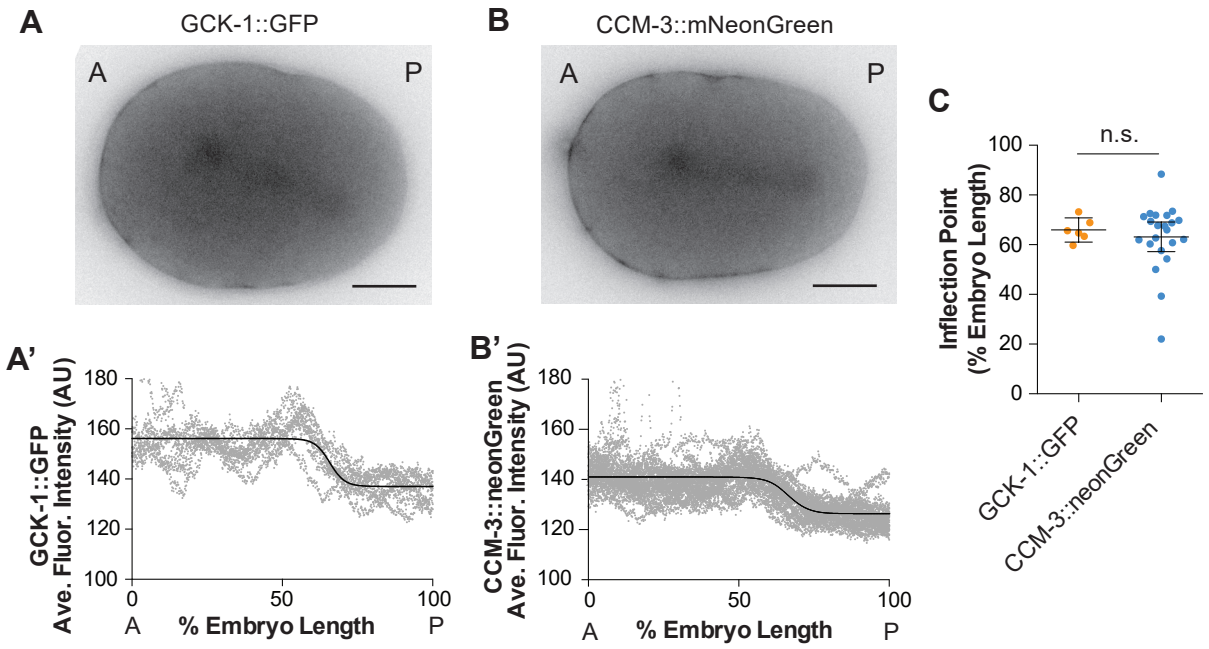

Figure 3

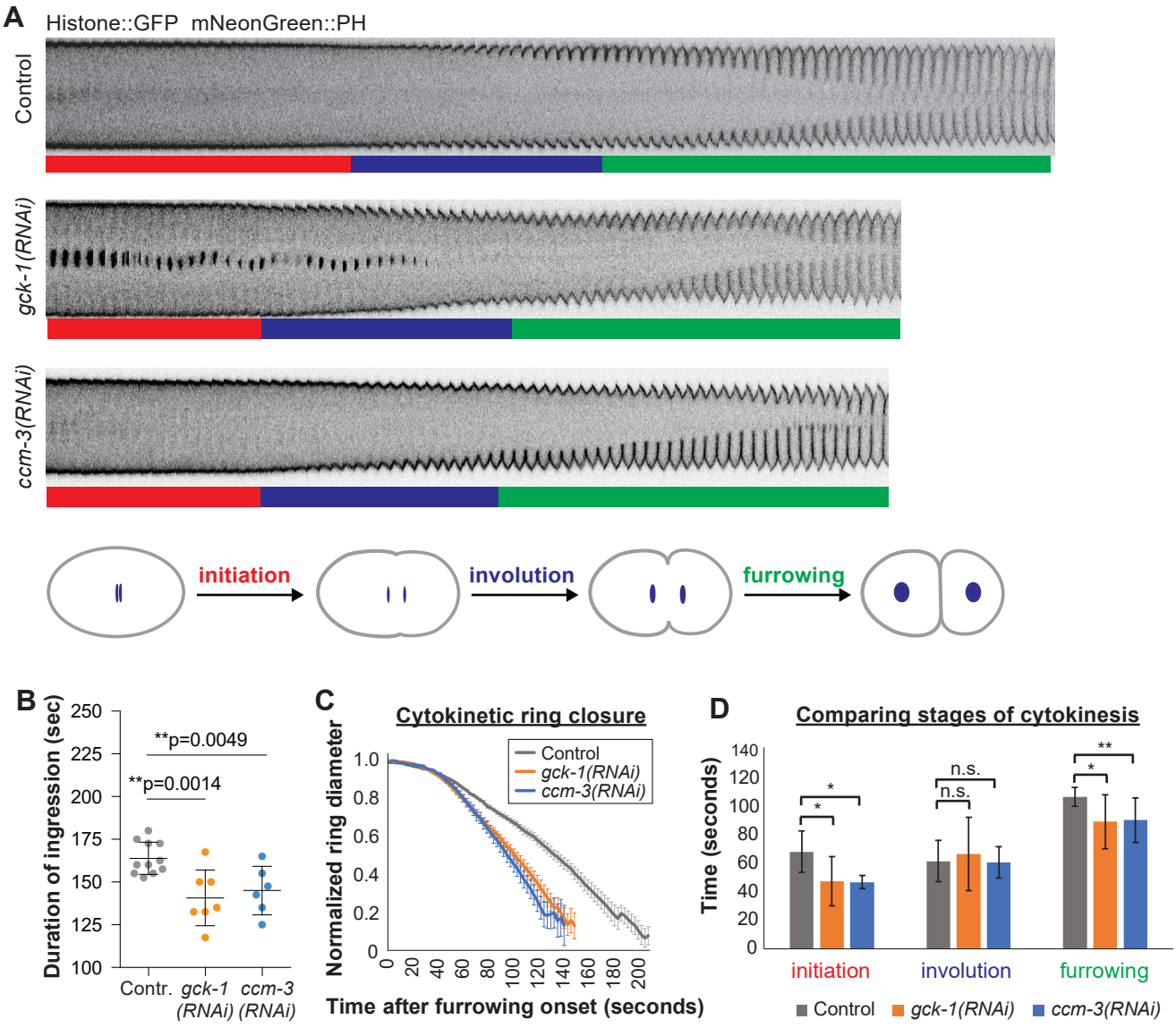

Figure 4

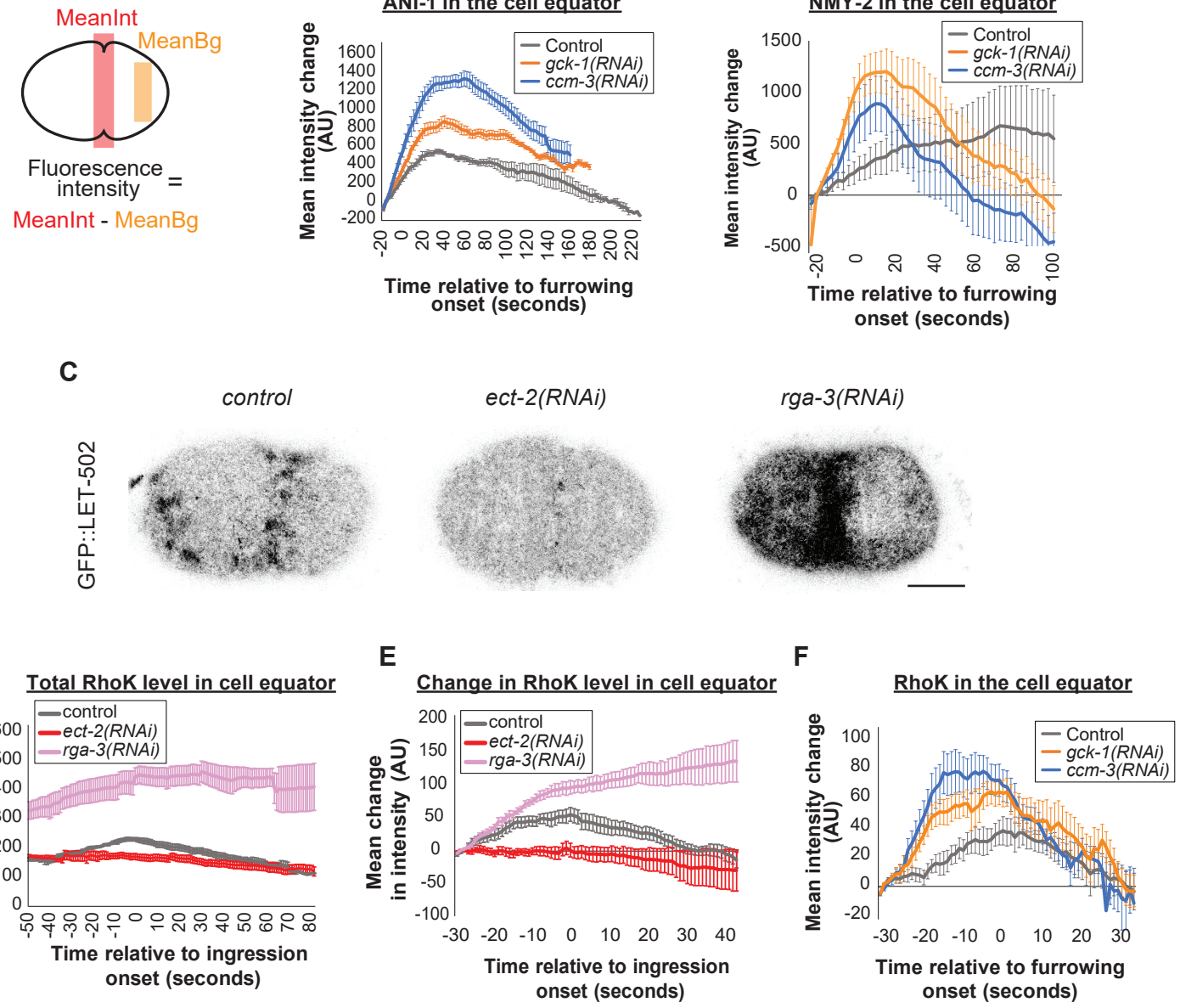

Figure 5

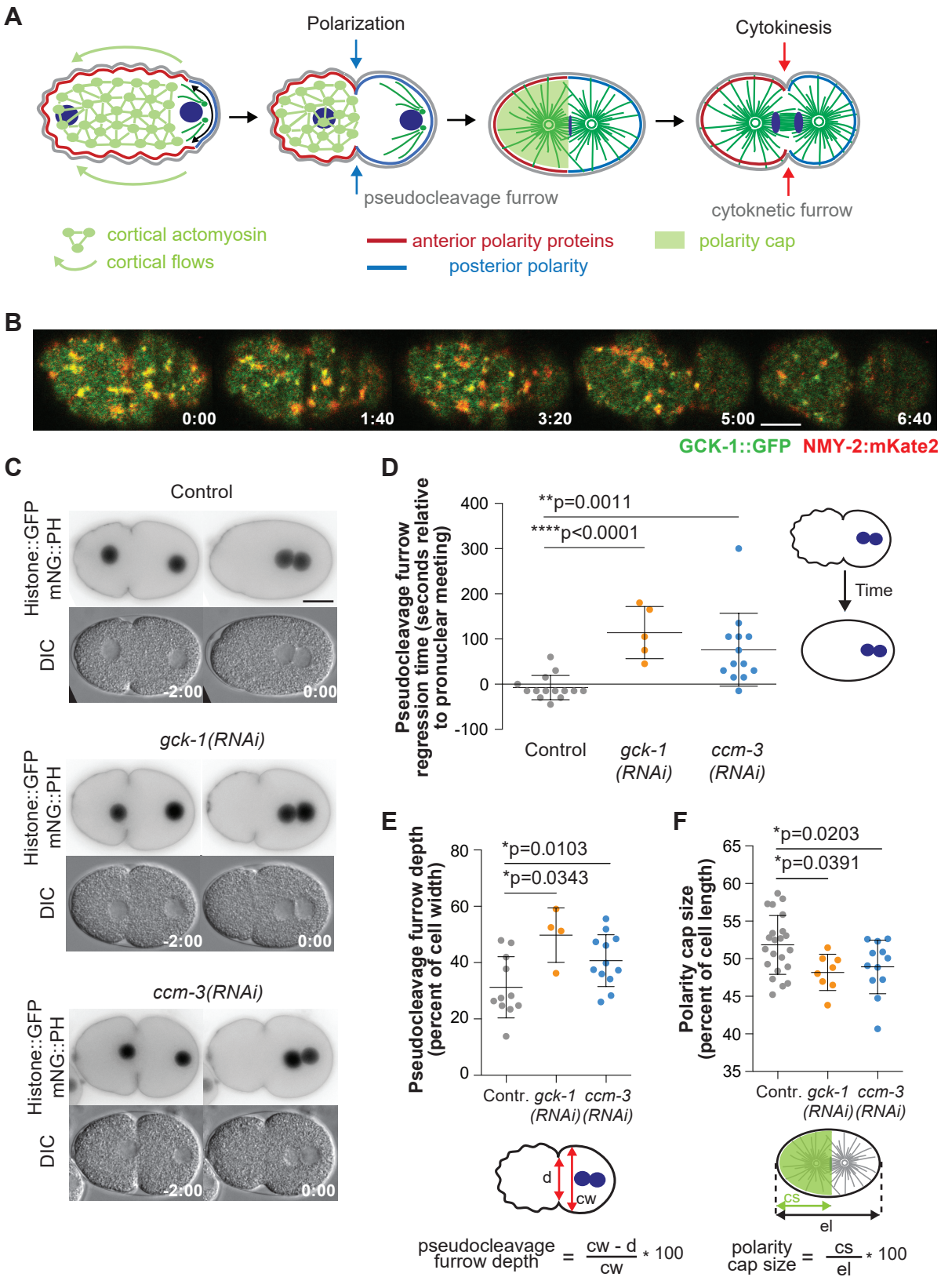

# Figure 5 Supplement

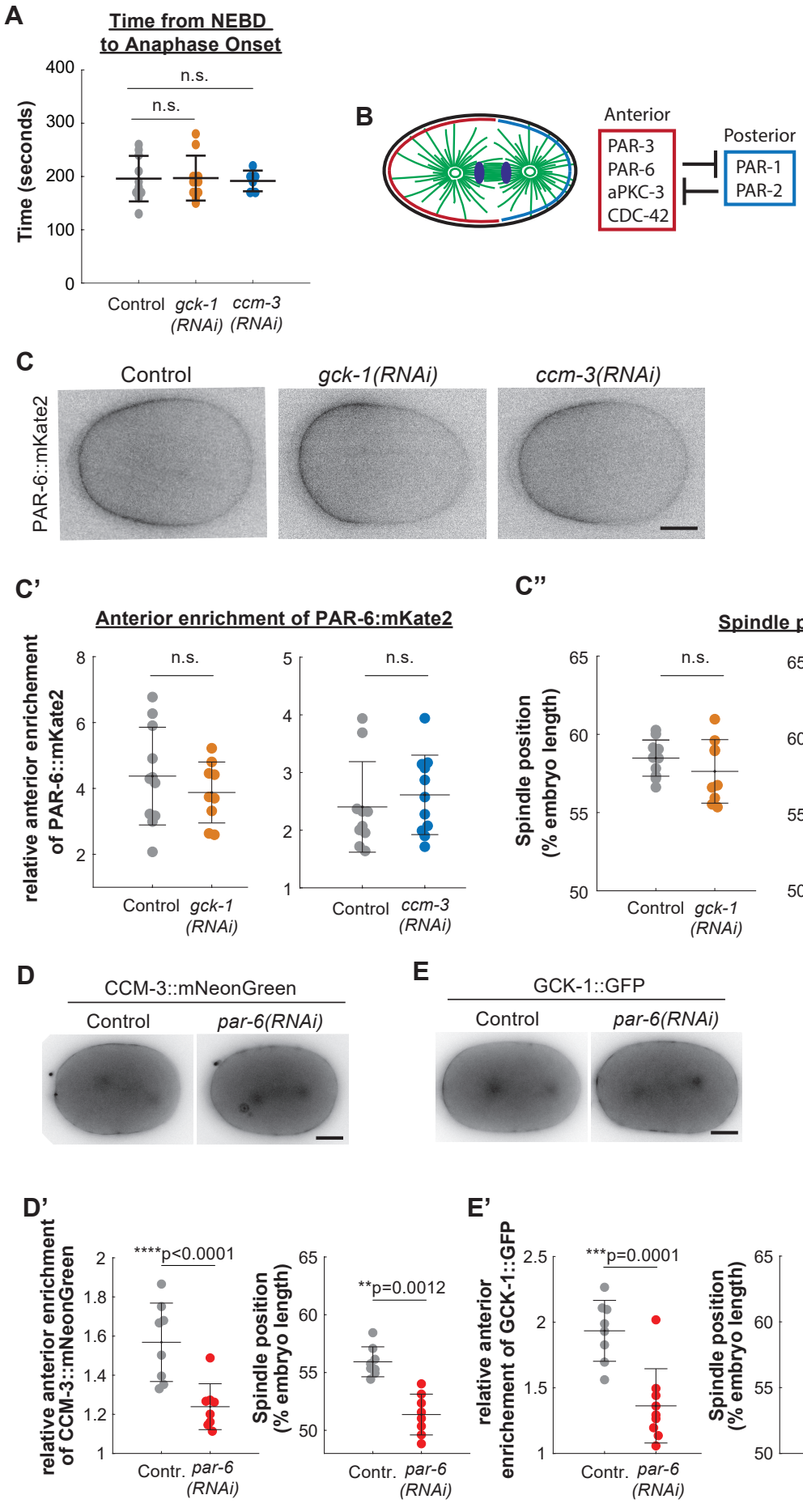

Figure 6

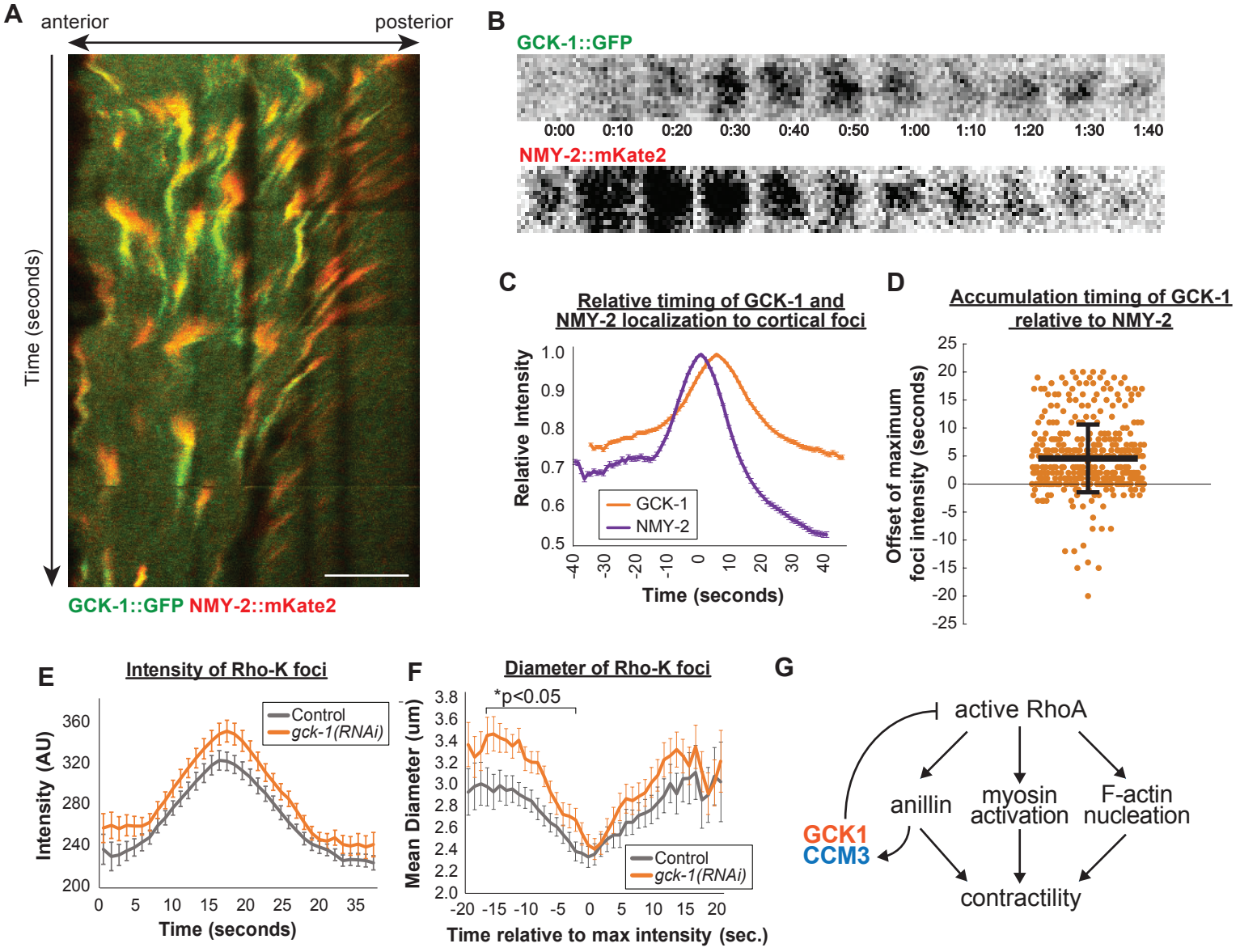


Figure 6

# Figure 6 Supplement